Heliyon 9 (2023) e17203

Contents lists available at ScienceDirect

Heliyon

journal homepage: www.cell.com/heliyon

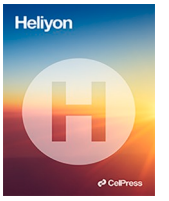

Spectral volume index creation and performance evaluation: A preliminary test for tree species identification

Huaipeng Liu

School of Land and Tourism, Luoyang Normal University, Luoyang, Henan Province, 471934, China

ARTICLE INFO

Keywords:
Four-seasonal RedEdge-MX data
Tree species identification
Spectral volume index creation
Performance evaluation
Random forest algorithm

ABSTRACT

To fully mine information regarding differences among various tree species from remote sensing data and improve the accuracy of tree species recognition, this study utilized the spectral reflection value, wavelength, and time as parameters and employed three algorithms to create an expression for the spectral volume index (SVI). Then, data were obtained by applying RedEdge-MX to four phases, SVI features were extracted, and a mixed feature set of spectral band + texture + digital surface model + SVI was constructed. A random forest algorithm was employed to determine the importance of the SVI features and derive the optimal feature set for tree species classification. The additional objectives were to determine if the SVI features have an active role in tree species classification and which algorithm is more conducive for extracting useful SVI features. The SVI features extracted with volume constraints exhibit better performance in tree species recognition than those extracted without volume constraints. Moreover, the SVI features extracted using a variable-constrained volume were better than those extracted using a constant-constrained volume. The combination of SVI features could improve the accuracy of tree species recognition (the highest overall accuracy was 92.76%), but the improvement effect was limited (the value was 92.16% when SVI features were not combined). These findings show that the SVI obtained using this method could be used to mine the difference information of tree species in images to a certain extent and hence, could be used in tree species identification.

1. Introduction

An important mode of forest resource investigation is to conduct a tree species survey. With the development of science and technology, researchers have attempted to use remote sensing (RS) technology to classify tree species and improve the technical level of forest resource investigation. This is because using RS technology to identify tree species can timely and accurately provide information regarding their growth status, composition structure, and spatial distribution at a large spatial scale. The acquisition of this information is crucial for practical applications, such as searching invasive tree species and ancient and famous trees, verifying afforestation, and monitoring tree species changes [1,2]. However, the problem of identifying tree species using RS technology still remains unsolved internationally [1]. At present, many scholars focus on in-depth explorations and research regarding this problem and strive to achieve a breakthrough. Solving this problem will have great practical significance for forest resource investigation, monitoring, and protection. First, it will change the traditional work mode of tree species surveys, which involves field sampling surveys, statistics, and reporting in grassroots units. Second, it will overcome the shortcomings of the traditional work mode, such as the requirement of considerable manpower as well as material and financial resources. Furthermore, it can quickly and accurately

E-mail address: huaipengliu985@163.com.

https://doi.org/10.1016/j.heliyon.2023.e17203
Received 23 November 2022; Received in revised form 8 June 2023; Accepted 9 June 2023
Available online 10 June 2023

extract the target forest tree species information, and spatial statistical analysis and visual analysis can be performed, which can improve the convenience and flexibility of forest resource investigation, monitoring, and protection. With the development of RS technology, aerospace and aerial sensors are constantly being upgraded and multiband, high-spatial-resolution RS data are emerging in large quantities [1]. With the advancement associated with computer-based classification methods and the progress of machine learning technology, more and more tree species are expected to be identified using RS technology; however, considerable difficulties are still present in accurately distinguishing tree species [3]. For example, the lack of spectral information with respect to RS data is a crucial factor contributing to this problem [1,4]. By creating new spectral features, deeply mining the difference information of tree species, and effectively compensating for the lack of spectral information with respect to RS data in tree species identification, an improvement in the accuracy of tree species recognition will play a positive role in promoting the application of RS technology in tree species recognition.

The research on tree species identification using RS technology has been ongoing for a long time. Gong et al. (1998) used the measured hyperspectral spectral data to identify tree species for the first time [5]. Later, with the development of aerospace and aviation RS technology, the research on tree species classification using image data gradually emerged. Notably, scholars have gradually transitioned from the identification of one tree species to the identification of multiple tree species [6,7]. For identifying multiple tree species, scholars have mainly conducted in-depth explorations on the selection of data sources and RS bands, considered temporal and multitype characteristic factors, and adopted and improved classification techniques. Furthermore, many valuable results have been obtained through such studies.

Scholars have used various types of data, such as IKONOS, QuickBird, LiDAR, WorldView-2/3, CASI, GeoEye, and unmanned aerial vehicle (UAV) aerial photography data, to select RS data sources and spectral bands (SBs). Some scholars have discussed the importance of IKONOS, WorldView-2, and WorldView-3 bands in tree species classification and selected some important bands conducive to tree species identification [8–12]. Furthermore, some scholars have discussed if combining data from multiple sources can effectively improve the accuracy of tree species recognition. For example, Cho et al. (2012) combined airborne spectral and LiDAR data [13]; Naidoo et al. (2012) integrated hyperspectral and LiDAR data [14]; Liu et al. (2013) combined hyperspectral CASI and airborne LiDAR data [15]; and Torabzadeh et al. (2019) combined imaging spectral and airborne laser scanning data to classify mixed forest tree species [16]. Thus, the effective combination of multisource data and the selection of key bands play a crucial role in tree species classification. In addition, hyperspectral imagery exhibits a better recognition ability in tree species identification than multispectral imagery [17–19].

With regard to time phase and feature type selection, many scholars confirmed that the use of one-period RS imagery fails to fully consider image changes caused by phenological changes in vegetation [20,21]. After noting this problem, some scholars introduced multitemporal RS data to focus on the reflection of phenological phenomena in RS data [22–26]. These scholars fully combined the features of different tree species in multitemporal images for classification. Their results show that seasonal effects have a strong influence on tree species discrimination and that using multiperiod RS images combinedly can improve the accuracy of tree species classification [27,28]. Some scholars combined SBs, spectral indices, texture features, color space features, height features, time-sequence features, and other multitype features of aerial photos and WorldView-3, airborne laser, and other multisource data to analyze the effect of tree species recognition [29–35]. Their studies reveal that an effective combination of multiple types and many features has a better classification effect than the use of one feature.

With regard to the use of classifiers, some scholars conducted research on the features of a support vector machine (SVM), object-oriented classification (OOC), a random forest (RF) algorithm, classified regression trees, and maximum-likelihood classification for tree species discrimination [36–40]. Their results show that SVMs, OOC, and RF algorithms have better performance than others, and an object-oriented SVM can achieve high recognition accuracy. With the introduction of machine learning in image classification [41–43] and in the feature selection and classification of high-dimensional data, XGBoost [44], LightGBM [45], and Softmax classification [42,46] methods are actively adopted owing to their superior performance compared to traditional methods. Tree species identification requires combining many features from multiple sources and multiphase RS data. Machine learning is actively used in research, and the accuracy of tree species identification has been effectively improved.

As evident from the literature review, in the research on the RS identification of tree species, scholars have considerably explored the selection of data sources, bands, imaging time phases, feature types, and classifiers; however, the mining of new features related to spectral indices is relatively lacking. Most existing studies have classified tree species by combining common spectral indices, such as NDVI, SAVI, EVI, ARVI, VARI, and CARI, with SBs, textures, and other features [2,9,47,48]. Additionally, some scholars have created a spectral area index and applied it to tree species classification [49,50]. Some studies have excluded the possibility of mistakenly extracting blue ground objects as vegetation in tree species classification by creating spectral indices that can extract them [41,51,52]. These studies show that the common vegetation index and new spectral area index are helpful for vegetation extraction and can improve the accuracy of tree species recognition. The spectral indices used previously in tree species classification were created through single or mixed operations, such as addition, subtraction, multiplication, and division between different bands. New spectral indices were later developed based on the slope and area differences formed by the spectral curves of different tree species in specific bands. Using the volume differences of cylinders formed by the spectral curves of different tree species in multitemporal RS images to obtain the latest spectral indices is now possible.

The reflectance spectrum curves of different tree species in multitemporal images should have certain differences in the volume of cylinders formed in a three-dimensional space [53]. Based on this, the author of the present study attempted to create spectral volume indices (SVIs) and test if their combination in a certain image feature set can improve the accuracy of tree species recognition. Herein, the spectral reflectance value, wavelength, and imaging time were used as parameters to create a spectral index that can express the volume of a columnar body formed by tree species in the spectral feature space. Additionally, RedEdge-MX images for four seasons

(spring, summer, autumn, and winter) were used as experimental data. Three algorithms were employed to calculate the volume of a cylinder under different constraints. The features extracted based on the SVI with SBs, textures, and digital surface models (DSMs) were combined. Then, an RF algorithm was employed to determine the importance ranking of all features and observe the ranking of SVIs in mixed feature sets (MFSs) and the number of selected features in optimal feature sets (OFSs) to comprehensively evaluate the performance of SVIs in tree species recognition. The research results will provide theoretical and methodological support for mining valuable image features of tree species identified using RS technology.

2. Materials and methods

2.1. Data acquisition and preprocessing

2.1.1. RedEdge-MX imagery

The study area is located on the new campus of Luoyang Normal University in Luoyang, Henan Province, China (Fig. 1(a)). The RS data used in this study were acquired using a UAV (RedEdge-MX sensor was mounted on a UAV JOUAV CW-15; the flight route and photo points of the UAV were designed using the ground station software JOUAV CWCommander, which was produced by China Chengdu Zongheng Automation Technology Co., Ltd.; the UAV flight height was ~370 m), and collected each season RS data have five SBs and one DSM [54]. Table 1 shows the detailed parameters of this sensor band setting, wavelength range, and spatial resolution (at the time of imaging). The RS data (Fig. 1) used in this study were imaged on March 15, 2021 (leafing and flowering periods) (Fig. 1(b)), September 29, 2020 (leafing period) (Fig. 1(c)), November 9, 2020 (leaf discoloration period) (Fig. 1(d)), and January 3, 2020 (late defoliation period) (Fig. 1(e)). Detailed data acquisition and preprocessing procedures can be found in a previous study [53].

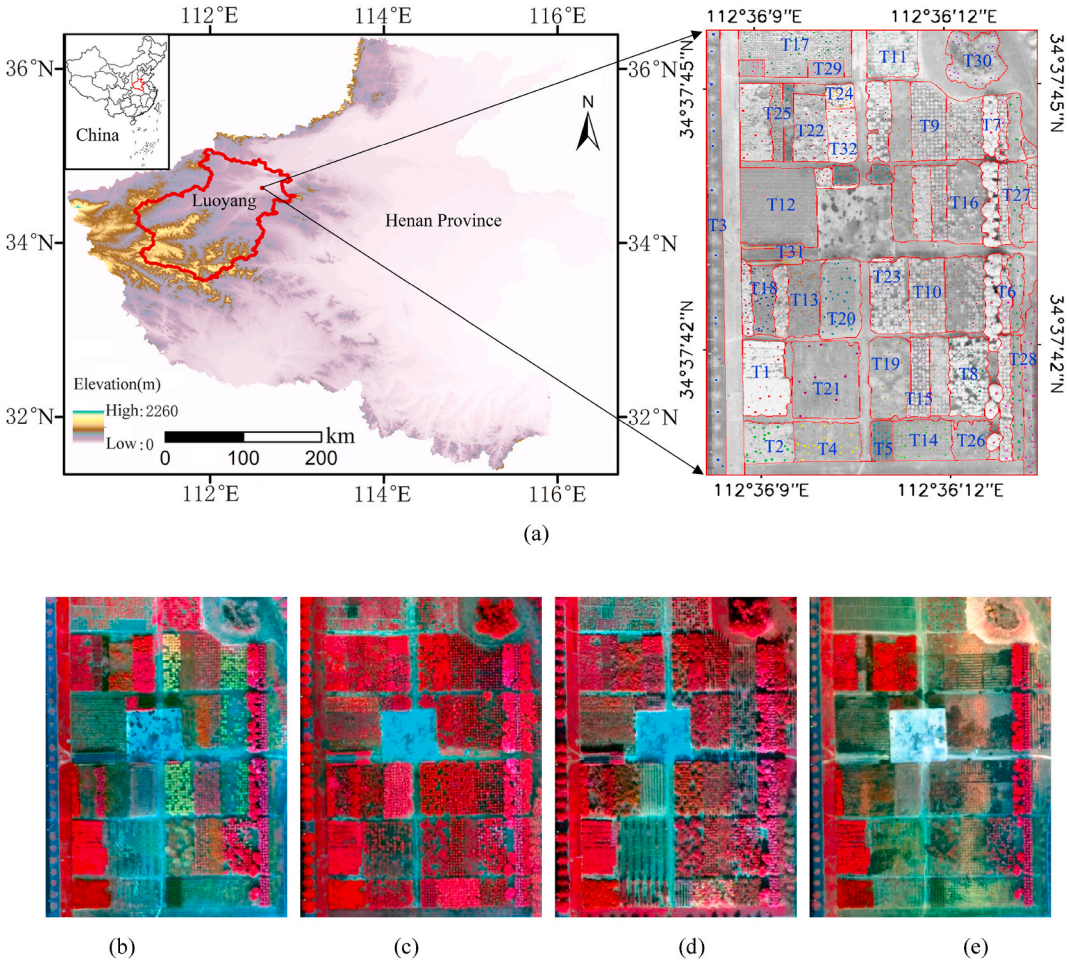

Fig. 1. Location map of the test area (~2.2 ha) and its four-seasonal imagery. (a) Location map of the test area; (b)–(e) spring, summer, autumn, and winter images, respectively, of the study area.

Table 1
Band, wavelength range, and spatial resolution information of the RedEdge-MX sensor.

Band number	Band name	Spatial resolution (cm)	Wavelength range (μm)	Central wavelength (μm)
1	Blue	15.00	0.465–0.485	0.475
2	Green		0.550–0.570	0.560
3	Red		0.663–0.673	0.668
4	Red edge		0.712–0.722	0.717
5	Near infrared		0.820–0.860	0.840

2.1.2. Tree species sample data

Between April and June 2021, tree species in the study area were surveyed in detail. During that time, the patches of the tree species were directly delineated, and their names were marked on RedEdge-MX printed images (standard false color). The outdoor tree species data collected were used to train and test tree species discrimination. In a laboratory, the tree species sample data were recorded in spreadsheets (Table 2) and converted into region of interest (ROI) files, which could be loaded on RedEdge-MX imagery for classification and verification. Detailed tree species survey and sample-collection procedures can also be found in a previous study [53]. All ROIs (right of Fig. 1(a)) and patches (Fig. 7(a)) of each tree species sample (for training and validation) were delineated on the corresponding images. The number of pixels for tree species classification and accuracy verification is shown in Table 2.

2.2. Methods

2.2.1. Creation of SVIs

In three-dimensional space, the spectral reflectance curves of the same tree species derived from spring, summer, autumn, winter, or additional time-series images will generally form a special prism with a fixed shape and volume. However, different types of tree species should have differences in the shape and volume of the prism obtained from the spectral curves of multiple time-series images. The creation and introduction of features that can express the prism volume difference of different tree species into tree species classification should improve the classification accuracy. Therefore, taking time (t), band (b), and reflectivity (r) as the three coordinate axes of a three-dimensional coordinate system, the prism formed by the spectral reflectance curve of the tree species could be constructed. As shown in Fig. 2(a), if the spectral reflectance curves of tree species 1 are T_1C_1 and T_2C_1 in T_1 and T_2 periods, respectively, the quadrangular prism formed by the two curves between bands B_1 and B_2 is A (T_1B_1–T_1B_2–T_2B_2–T_2B_1–R_{21}–R_{11}–R_{12}–R_{22}). Moreover, the quadrangular prism of tree species 2 formed by curves T_1C_2 and T_2C_2 between bands B_1 and B_2 is T_1B_1–T_1B_2–T_2B_2–T_2B_1–r_{21}–r_{11}–r_{12}–r_{22}. The volume of the quadrangular prism formed by the spectral reflectance curves between the two bands of the two tree species is different. From this perspective, we can construct an SVI that can mine the difference information of various tree species in images.

In Fig. 2(a), taking tree species 1 as an example, quadrangular prism A can be disassembled into triangular prisms B

Table 2
Scientific names of each tree species and numbers of pixels for tree species classification and accuracy verification.

Tree species number	Scientific names	Training samples	Validation samples	Tree species number	Scientific names	Training samples	Validation samples
T1	*Photinia × fraseri*	238	32,400	T17	*Paeonia suffruticosa*	237	23,733
T2	*Loropetalum chinense* var. *Rubrum*	257	11,437	T18	*Acer serrulatum*	202	8560
T3	*Platanus orientalis*	238	33,840	T19	*Armeniaca mume* f. *Rubriflora*	226	34,120
T4	*Armeniaca vulgaris*	230	14,538	T20	*Acer negundo "Aurea"*	231	17,933
T5	*Punica granatum "Flavescens"*	274	14,476	T21	*Cerasus avium*	207	28,549
T6	*Cedrus deodara*	235	20,098	T22	*Nandina domestica*	353	17,129
T7	*Cinnamomum camphora*	262	24,080	T23	*Prunus × blireana "Meiren"*	230	25,496
T8	*Magnolia grandiflora*	206	16,593	T24	*Viburnum odoratissimum*	220	3967
T9	*Malus micromalus*	242	33,414	T25	*Ligustrum quihoui*	232	7168
T10	*Chaenomeles cathayensis*	263	20,711	T26	*Crataegus pinnatifida*	218	7946
T11	*Osmanthus fragrans* var. *Semperflorens*	148	13,288	T27	*Bischofia polycarpa*	311	27,136
T12	*Rosa chinensis*	223	32,708	T28	*Koelreuteria paniculata*	255	13,973
T13	*Acer palmatum "Atropurpureum"*	231	13,283	T29	*Paeonia lactiflora*	132	5691
T14	*Aesculus chinensis*	238	13,582	T30	*Populus tomentosa*	243	14,752
T15	*Malus halliana*	247	16,280	T31	*Wisteria sinensis*	213	3772
T16	*Michelia champaca*	279	47,974	T32	*Climbing Roses*	229	11,859

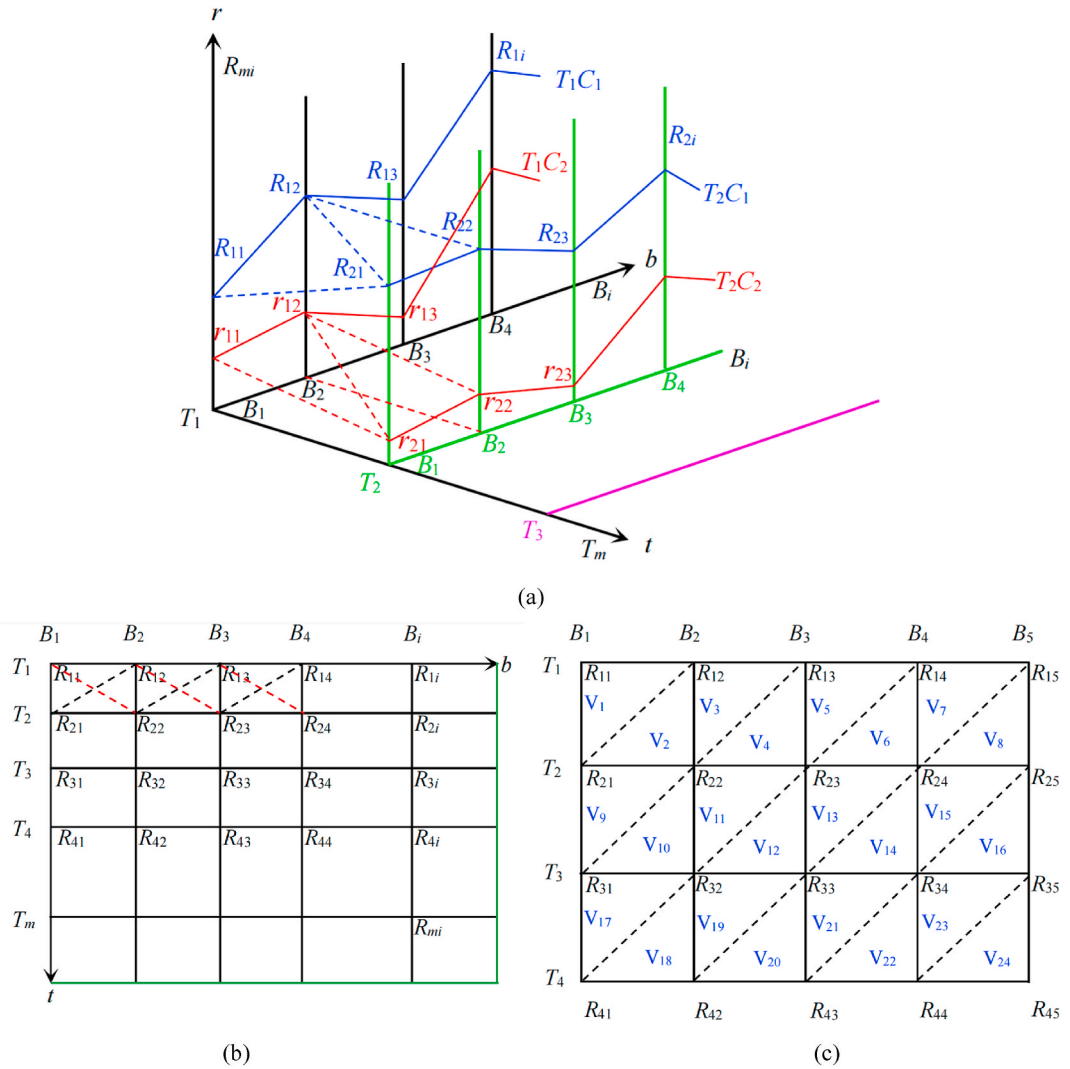

Fig. 2. Schematic of spectral volume index (SVI) construction and illustration of SVI extraction. (a) Schematic of the volume difference of prisms formed by the spectral reflectance curves of different tree species. (b) Schematic of connecting the projection points of spectral reflectance values in the form of main (sub) diagonal lines. (c) SVI explanatory diagram extracted in this study.

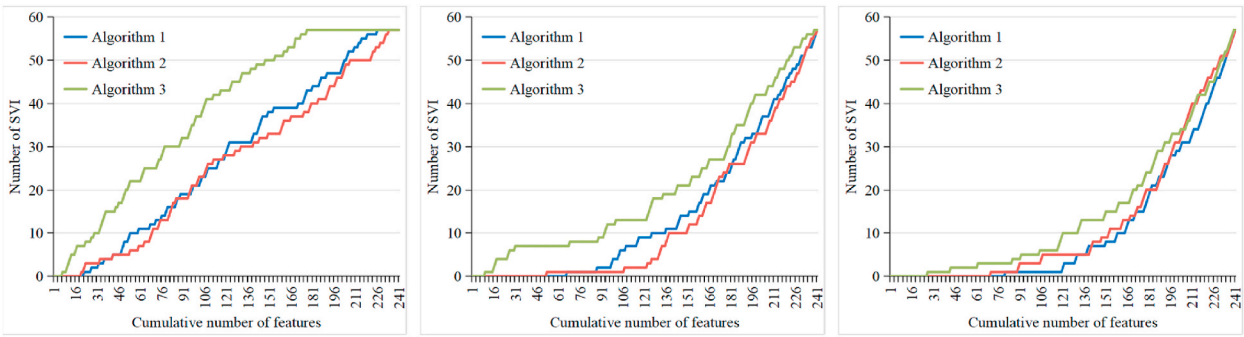

Fig. 3. Cumulative distribution of SVIs extracted using the three algorithms in the total feature set under different texture extraction windows. (a) Under a 3 × 3 window; (b) under a 9 × 9 window; and (c) under a 43 × 43 window.

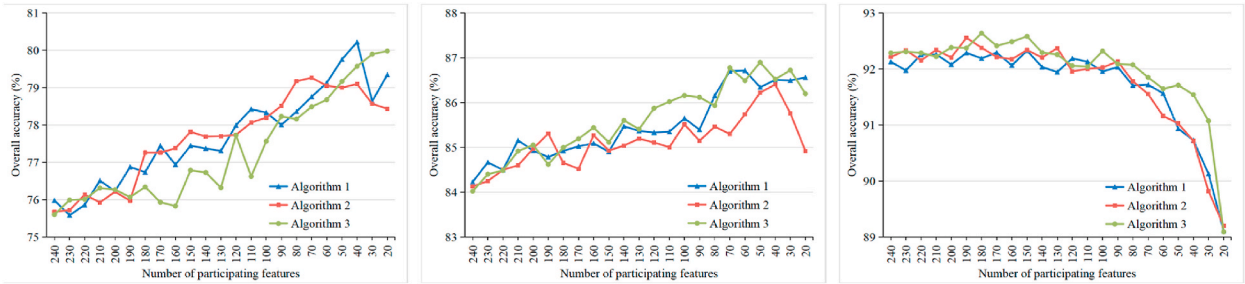

Fig. 4. Number of features involved and overall accuracy change of tree species identification when ten features were eliminated each time. (a) Under a 3 × 3 window; (b) under a 9 × 9 window; and (c) under a 43 × 43 window.

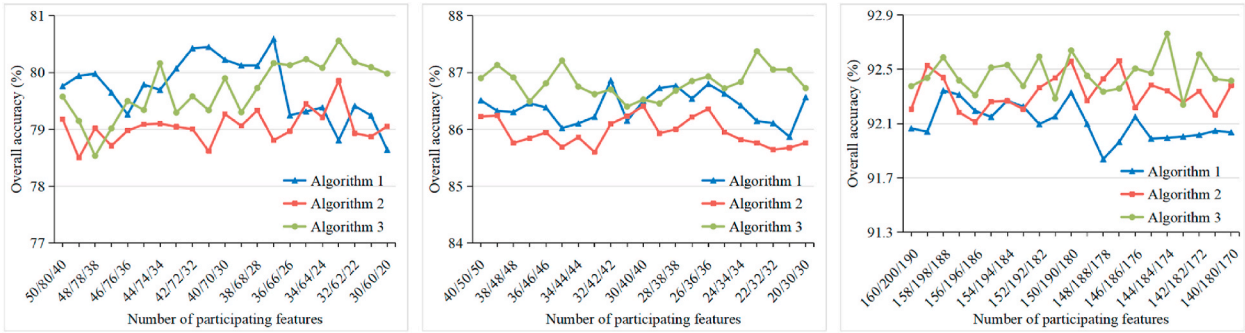

Fig. 5. Number of features involved and the overall accuracy change of tree species discrimination when one feature was eliminated each time. (a) Under a 3 × 3 window; (b) under a 9 × 9 window; and (c) under a 43 × 43 window.

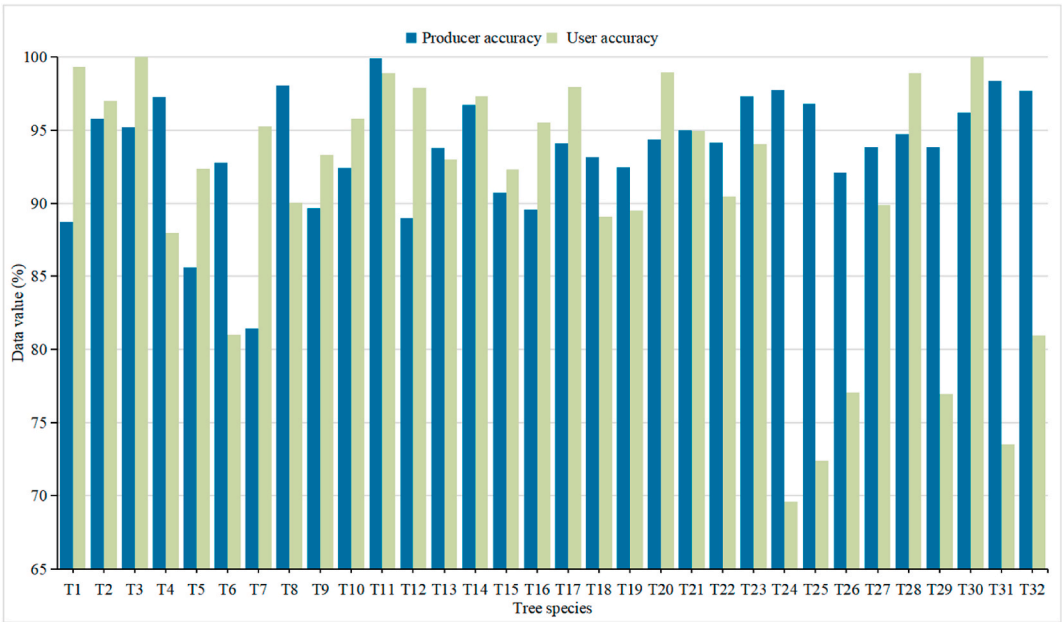

Fig. 6. Producer and user accuracy histograms of the best discrimination results.

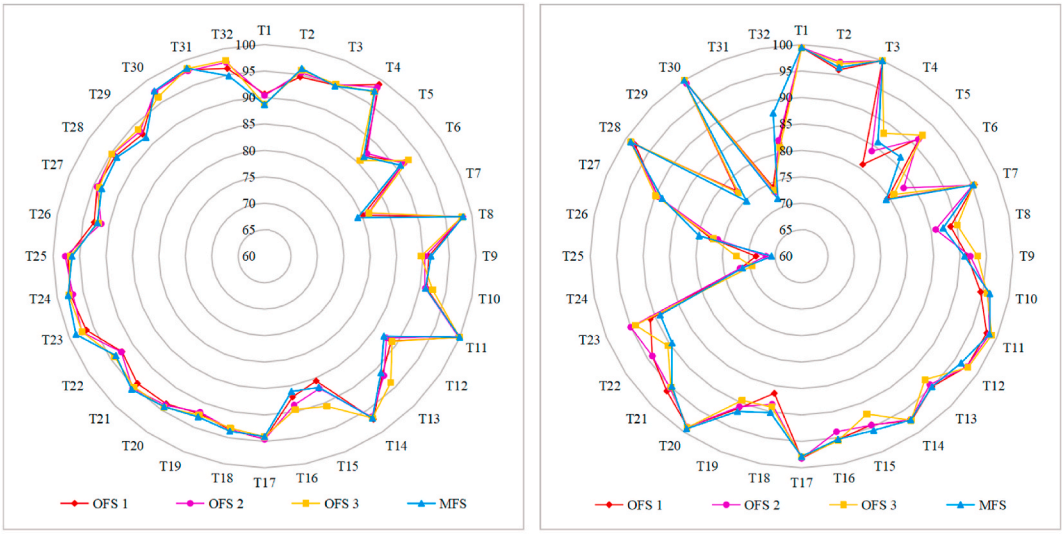

Fig. 7. Spider-web graphs of the OFS 1, OFS 2, OFS 3, and MFS classification results. (a) Graph of producer accuracies and (b) graph of user accuracies.

(T_1B_1–T_1B_2–T_2B_1–R_{21}–R_{11}–R_{12}) and C (T_1B_2–T_2B_2–T_2B_1–R_{21}–R_{12}–R_{22}). We determine the volumes of the two triangular prisms separately and then add them together to obtain the volume of quadrangular prism A (Eq. (3)). The volumes of triangular prisms B and C can be obtained using Eqs. (1) and (2), respectively.

$$V_B = \frac{1}{3} \times \left(\frac{1}{2} \times \Delta t_{12} \times \Delta \lambda_{12} \right) \times (R_{11} + R_{12} + R_{21}) = \frac{1}{6} \times \Delta t_{12} \times \Delta \lambda_{12} \times (R_{11} + R_{12} + R_{21}) \tag{1}$$

$$V_C = \frac{1}{3} \times \left(\frac{1}{2} \times \Delta t_{12} \times \Delta \lambda_{12} \right) \times (R_{12} + R_{22} + R_{21}) = \frac{1}{6} \times \Delta t_{12} \times \Delta \lambda_{12} \times (R_{12} + R_{22} + R_{21}) \tag{2}$$

$$V_A = V_B + V_C = \frac{1}{6} \times \Delta t_{12} \times \Delta \lambda_{12} \times (R_{11} + 2 \times (R_{12} + R_{21}) + R_{22}) \tag{3}$$

where Δt_{12} represents the time difference between T_2 and T_1, $\Delta\lambda_{12}$ represents the center wavelength difference between bands B_2 and B_1, R_{11} and R_{12} are the reflectances of tree species 1 on bands B_1 and B_2, respectively, at T_1 phase, and R_{21} and R_{22} are the reflectances of tree species 1 on bands B_1 and B_2, respectively, at T_2 phase.

When viewed vertically downward from the top surface of Fig. 2(a), the projection of the spectral reflectance value points of the tree species is shown in Fig. 2(b). The corresponding projection points are successively connected in the form of subdiagonal lines (lower left to upper right; black dotted lines in the figure). The volume of each quadrangular prism is first calculated separately, and then, all such volumes are added to obtain a unified model of the SVI formed by the spectral reflectance curve of multitemporal tree species in the three-dimensional space, as shown in Eq. (4). The corresponding projection value points are successively connected in the form of a main diagonal line (upper left to lower right; red dotted lines in the figure). The unified model of the SVI created in this form is shown in Eq. (5). Although formulas (4) and (5) are similar, they are fully equivalent only when $R_{mj} + R_{ni} = R_{mi} + R_{nj}$.

$$SVI_1 = \frac{1}{6} \times \sum_{m=1}^{K-1} \Delta t_{mn} \times \sum_{i=1}^{N-1} \Delta \lambda_{ij} \times \left(R_{mi} + 2 \times \left(R_{mj} + R_{ni} \right) + R_{nj} \right) \tag{4}$$

$$SVI_2 = \frac{1}{6} \times \sum_{m=1}^{K-1} \Delta t_{mn} \times \sum_{i=1}^{N-1} \Delta \lambda_{ij} \times \left(R_{mj} + 2 \times \left(R_{mi} + R_{nj} \right) + R_{ni} \right) \tag{5}$$

where SVI is the spectral volume index; K is the total number of RS data used; $m = 1, 2, 3, \ldots, K-1$; N is the band number of RS data; and $i = 1, 2, 3, \ldots, N-1$ with $j = i + 1$. R_{mi} is the spectral reflectance value of the ith band in the m-phase, R_{mj} is the spectral reflectance value of the $(i+1)$th band in the m-phase, R_{ni} is the spectral reflectance value of the ith band in the $m+1$ phase, R_{nj} is the spectral reflectance value of the $(i+1)$th band in the $m+1$ phase, $\Delta\lambda_{ij}$ is the difference in the center wavelengths of the j- and i-band, and Δt_{mn} is the time difference between the n- and m-phase.

Furthermore, to increase the volume difference of the prism formed by the spectral reflectance curves of different tree species, the volume of the regular triangular prism, whose height is the smallest spectral reflectance value among all the tree species, was sub-

tracted from the prism to enhance the contrast. When the volume of the regular triangular prism is calculated by multiplying the height C (a constant) with the base area, the unified model of the SVI is obtained as per Eq. (6). When the volume of the regular triangular prism is calculated by multiplying the height B_m (a variable) with the base area, the unified model of the SVI is obtained as per Eq. (7).

$$SVI_3 = \frac{1}{6} \times \sum_{m=1}^{K-1} \Delta t_{mn} \times \sum_{i=1}^{N-1} \Delta \lambda_{ij} \times \left(R_{mj} + 2 \times \left(R_{mi} + R_{nj}\right) + R_{ni} - 3 \times C\right) \tag{6}$$

$$SVI_4 = \frac{1}{6} \times \sum_{m=1}^{K-1} \Delta t_{mn} \times \sum_{i=1}^{N-1} \Delta \lambda_{ij} \times \left(R_{mj} + 2 \times \left(R_{mi} + R_{nj}\right) + R_{ni} - 3 \times B_m\right) \tag{7}$$

2.2.2. Extraction of SVI features

Following the abovementioned construction strategy, the projection points of tree species spectral reflectance value points in the 5-band RedEdge-MX data in four time periods can be obtained, as shown in Fig. 2(c). Connecting nonadjacent projection points in a subdiagonal form (this form is discussed in this study) can divide Fig. 2(c) into 24 triangular regions. Using Eq. (4) to extract SVI features (the time interval between adjacent time phase data is calculated in units of 1), 24 triangular prisms (V_1–V_{24}) can be first extracted. Second, the quadrangular prism $V_1 + V_2$ formed between bands 1 and 2 of the spring and summer data (summer and autumn; autumn and winter) is named $V_{sp\text{-}su\ 1\text{–}2}$. In this manner, bands 1 to 3, 4, and 5 (bands 2 to 3, 4, and 5; bands 3 to 4 and 5; bands 4 and 5) are obtained in turn to form the quadrangular prism volume, and 30 SVI features can be obtained. Third, the quadrangular prisms $V_{sp\text{-}su\ 1\text{–}5}$, $V_{su\text{-}au\ 1\text{–}5}$, and $V_{au\text{-}wi\ 1\text{–}5}$ are added to obtain three SVI features (i.e., $V_{sp\text{-}su\text{-}au\ 1\text{–}5}$, $V_{sp\text{-}su\text{-}au\text{-}wi\ 1\text{–}5}$, and $V_{su\text{-}au\text{-}wi\ 1\text{–}5}$). Based on the abovementioned three SVI feature extraction forms, 57 SVIs can be obtained. According to Eqs. (6) and (7), each algorithm can extract 57 SVI features. This study mainly compares the performance of SVIs extracted using the three algorithms in tree species classification. During the calculation of the volume of a single triangular prism, the constant C and variable B_m were used according to the statistical results shown in Table 3.

2.2.3. Mask construction and auxiliary feature extraction

To verify the performance of the newly created SVI in tree species classification, a mask was first constructed to cover the nontree part of the image during tree species discrimination, and only the tree part of the image was retained for participation in the calculation. Then, an MFS (20 SBs + 160 textures (TEXs) + 4 DSMs) was constructed. The SB comprised 5-band images in four seasons, including 20 bands, while the DSM comprised one DSM in each season, including four DSM features. Texture features comprised mean, variance, homogeneity, contrast, dissimilarity, entropy, second moment, and correlation extracted from 20 bands, including 160 features. After constructing the MFS, the extracted SVI features were combined with the feature set, the importance of all features was sorted using the RF algorithm, and the performance of SVI features in tree species discrimination was analyzed. The mask construction and TEX extraction were the same as those in a previous study [53]. As the window size used for texture extraction affects the classification accuracy of the image, the texture extraction windows with the minimum (3 × 3), middle (9 × 9), and highest (43 × 43) tree species classification accuracies were selected for analysis [53]. Moreover, changes in the importance of SVI features were compared and analyzed as the texture performance was enhanced in tree species classification.

2.2.4. Image classification and OFS determination

The feature sets of MFSs combined with SVI features (MFSs + 57 SVIs) and the SVI feature set (57 SVIs) were used as image feature sets for tree species recognition. Considering that these two types of feature sets are high-dimensional datasets, they will affect the classification performance of classifiers. Thus, a strong correlation was observed between SVI and 20 S B features, which would affect the evaluation of the importance of SVI features in the classification results. Therefore, classifiers that are insensitive to feature

Table 3
Values of the constant C and variable B_m of a single triangular prism SVI extracted by different band combinations.

SVIs of the triangular prism	Constant C	Variable B_m	SVIs of the triangular prism	Constant C	Variable B_m
V_1	0.09283	Summer b_1	V_{13}	0.08652	Summer b_3
V_2	0.09283	Summer b_1	V_{14}	0.09762	Autumn b_3
V_3	0.10796	Summer b_2	V_{15}	0.18564	Summer b_4
V_4	0.08652	Summer b_3	V_{16}	0.20664	Autumn b_4
V_5	0.08652	Summer b_3	V_{17}	0.09745	Autumn b_1
V_6	0.08652	Summer b_3	V_{18}	0.09988	Autumn b_2
V_7	0.18564	Summer b_4	V_{19}	0.09762	Autumn b_3
V_8	0.18564	Summer b_4	V_{20}	0.09762	Autumn b_3
V_9	0.09283	Summer b_1	V_{21}	0.09762	Autumn b_3
V_{10}	0.09745	Autumn b_1	V_{22}	0.13953	Winter b_3
V_{11}	0.08652	Summer b_3	V_{23}	0.20664	Autumn b_4
V_{12}	0.08652	Summer b_3	V_{24}	0.24432	Autumn b_5

Notes: Summer b_1, Autumn b_1, and Winter b_3 represent RedEdge-MX band 1 of summer data, band 1 of autumn data, and band 3 of winter data, respectively. For other such terms, one can refer to the above three explanations for understanding. In addition, the constant C and its corresponding variable B_m were determined from the statistics of the training samples of 32 tree species.

dimensionality and correlation must be selected. An RF algorithm was selected for all experiments involved in the SVI evaluation because of its excellent performance in high-dimensional data classification and feature importance ranking. The classification and feature ranking tool was EnMAP-Box [55].

When the tree species classification using the abovementioned feature sets was completed, the importance of features in the MFSs + SVIs was measured, and the OFSs for each MFS + SVI were obtained. First, the importance of features according to the normalized importance value was ranked from 1 to 241. Then, starting from MFSs + SVIs containing 240 features, the tree species were classified in a decreasing form for every ten participating features, and the overall accuracy was recorded to obtain the feature set with the highest accuracy (the number of participating features was recorded as *N*). Next, the features were sorted according to their importance and were eliminated one by one within the range of feature participation numbers from $N - 10$ to $N + 10$. The overall accuracy was recorded, and the corresponding classification feature set was determined when the overall accuracy was the highest; it was determined as the best feature set for tree species identification.

2.2.5. SVI performance evaluation

The importance of SVI features in tree classification and appropriate calculation methods was evaluated from three aspects: the cumulative distribution of SVI features in new MFSs, the number of selected SVI features in the OFSs, and the difference in the classification accuracy of SVI feature sets for tree species obtained using the three algorithms. The classification results of the MFSs, whose textures were extracted from 3 × 3, 9 × 9, and 43 × 43 window sizes, were used as a reference to compare and analyze the experimental results of this study.

Table 4
Status of SVIs extracted using the three algorithms (Algs.) in the optimal feature set under three types of texture extraction windows.

Window size for texture extraction	3 × 3			9 × 9			43 × 43		
	Alg. 1	Alg. 2	Alg. 3	Alg. 1	Alg. 2	Alg. 3	Alg. 1	Alg. 2	Alg. 3
Total number of features contained in the OFS	37	63	23	32	40	33	158	187	174
Number of SVI features in the OFS	4	7	8	0	0	7	9	21	21
Selected SVI features (sorted by a decreasing importance value)	V_{16}	V_{24}	V_{11}			$V_{su\text{-}au\ 1–2}$	V_{18}	V_{07}	V_{02}
	V_{05}	V_{05}	V_{02}			V_{11}	V_{20}	V_{24}	V_{16}
	$V_{au\text{-}wi\ 4–5}$	V_{22}	V_{23}			V_{10}	V_{10}	V_{04}	$V_{su\text{-}au\ 1–3}$
	V_{23}	$V_{au\text{-}wi\ 4–5}$	V_{16}			V_{02}	V_{14}	$V_{sp\text{-}su\ 4–5}$	V_{11}
		V_{10}	$V_{su\text{-}au\ 1–2}$			$V_{su\text{-}au\ 1–3}$	V_{05}	V_{18}	$V_{sp\text{-}su\text{-}au\ 1–5}$
		V_{16}	$V_{su\text{-}au\ 1–3}$			V_{19}	$V_{su\text{-}au\ 1–3}$	V_{10}	$V_{su\text{-}au\ 2–5}$
		$V_{au\text{-}wi\ 2–5}$	V_{15}			V_{17}	$V_{sp\text{-}su\ 4–5}$	V_{09}	$V_{su\text{-}au\ 4–5}$
			V_{10}				V_{02}	V_{08}	$V_{su\text{-}au\ 1–2}$
							$V_{sp\text{-}su\ 1–2}$	V_{19}	V_{23}
								$V_{sp\text{-}su\ 2–5}$	V_{19}
								$V_{sp\text{-}su\ 2–3}$	V_{17}
								$V_{sp\text{-}su\ 1–2}$	V_{08}
								V_{05}	V_{04}
								$V_{au\text{-}wi\ 1–5}$	$V_{sp\text{-}su\ 1–3}$
								$V_{au\text{-}wi\ 2–5}$	V_{20}
								V_{12}	$V_{sp\text{-}su\ 2–3}$
								$V_{au\text{-}wi\ 2–3}$	V_{10}
								$V_{sp\text{-}su\ 3–4}$	$V_{su\text{-}au\ 3–5}$
								V_{06}	$V_{sp\text{-}su\ 4–5}$
								V_{03}	V_{14}
								$V_{sp\text{-}wi\ 1–5}$	V_{18}

3. Results and analyses

3.1. Cumulative distribution of SVI features

In tree species classification, the cumulative distribution of SVIs extracted using the three algorithms in the MFSs + SVIs (160 TEXs (extracted under different scale windows) + 20 SBs + 4 DSMs + 57 SVIs) is shown in Fig. 3(a) and (c).

As shown in Fig. 3(a) and (c), with the increase of texture extraction windows in tree species recognition, the cumulative distribution of SVIs extracted using the three algorithms in the feature sets of MFSs + SVIs gradually changes from a relatively front distribution to a rear distribution. Regardless of the scale window used to extract texture, the cumulative distribution of SVIs extracted using algorithm 3 in the feature sets of MFSs + SVIs was more forward than those extracted using the other algorithms. The SVIs extracted using algorithms 2 and 3 have similar distributions in the MFS + SVI feature sets (textures derived from different extraction windows).

3.2. Optimal feature participation number in tree species classification

Fig. 4(a) and (c) shows the overall accuracy change of tree species recognition in which the feature participation number was between 20 and 240, and 10 features were eliminated each time. Fig. 5(a) and (c) shows the participation number range of the most suitable quantitative features for tree species discrimination and the overall accuracy change of the tree species discrimination with one feature eliminated each time.

As shown in Fig. 4(a)-(c), with the gradual reduction of participating features, the overall accuracy of tree species discrimination first rises and then begins to decline. When the size of the texture extraction window was small (i.e., 3 × 3 and 9 × 9), a few participating features can make tree species classification achieve high overall accuracy (Fig. 4(a) and (b)). In contrast, when the size of the texture extraction window was large (under a 43 × 43 window), the high accuracy of tree species recognition was determined by the participation of many features (Fig. 4(c)).

Under the 3 × 3, 9 × 9, and 43 × 43 windows, the numbers of features in the best feature set in tree species discrimination for the MFSs + SVIs constructed using the three algorithms were approximately 40, 70, and 30; 30, 40, and 40; and 150, 190, and 180, respectively.

As can be seen from the more detailed feature elimination process (Fig. 5(a)-(c)), in a small-scale window (e.g., 3 × 3 and 9 × 9), the MFSs + SVIs constructed using algorithms 1 and 3 exhibit better performance in tree species classification than those constructed using algorithm 2 (i.e., in most cases, the overall tree species identification accuracy of algorithms 1 and 3 was higher than that of algorithm 2) (Fig. 5(a) and (b)). However, under the optimal texture extraction window (43 × 43), the MFSs + SVIs constructed using algorithms 2 and 3 outperformed those constructed using algorithm 1 in tree species classification (Fig. 5(c)). Based on Figs. 4 and 5, regardless of which window scale was used to extract texture, the feature set MFS + SVIs constructed using algorithm 3 has satisfactory performance in tree species classification.

3.3. Status of SVIs in the OFS

The selected numbers and feature names of SVIs extracted using the three algorithms in the OFSs of tree species discrimination are shown in Table 4.

In Table 4, when the 3 × 3 and 43 × 43 windows were used for texture extraction, the SVIs calculated using the three algorithms were selected in the OFSs. Conversely, when the processing window used for texture extraction was 9 × 9, only the SVI features calculated using algorithm 3 were selected in the OFS. The number of features contained in the OFS for tree species classification obtained by extracting texture under a large window (43 × 43) was more than that in the OFS obtained by extracting texture under the small windows (3 × 3 and 9 × 9). Correspondingly, under the optimal texture extraction window, the number of SVI features involved in the OFS was more than that involved in the OFS when the textures were extracted under the small windows.

The overall accuracies of the MFSs + SVIs, OFSs of the MFSs + SVIs, and MFSs for tree species classification are shown in Table 5.

From Table 5, the overall accuracies of the OFSs for tree species classification were higher than their parent feature sets MFSs + SVIs and the smaller the windows for texture extraction, the more obvious the difference in their accuracy. The overall accuracy of the OFS with the participation of the SVI calculated using algorithm 3 for tree species discrimination was higher than that of the OFS with the participation of the SVI calculated using the other two algorithms. Using MFSs for tree species discrimination, the maximum accuracies of tree species recognition were 79.38%, 84.82%, and 92.16%. However, when the SVIs extracted using the three

Table 5
Accuracy difference between the mixed feature set and optimal feature set constructed using the three algorithms in tree species recognition under different texture extraction windows.

Window size for texture extraction	SVI calculated using Alg. 1		SVI calculated using Alg. 2		SVI calculated using Alg. 3		MFSs
	MFS + SVIs	OFS 1	MFS + SVIs	OFS 2	MFS + SVIs	OFS 3	
3 × 3	75.95	80.59	75.98	79.85	75.42	80.56	79.38
9 × 9	84.04	86.86	84.20	86.41	83.73	87.37	84.82
43 × 43	92.18	92.34	92.55	92.56	92.44	92.76	92.16

algorithms were combined, the accuracy of tree species discrimination exceeded that of the combination of the three types of features.

3.4. Only SVI features were used for tree species discrimination

By only using the SVI features extracted using the three algorithms to classify tree species, the obtained overall accuracies and Kappa coefficients are shown in Table 6.

As shown in Table 6, the accuracy of the SVI features extracted using algorithm 2 for tree species classification was slightly higher than that extracted using algorithm 1. The accuracy of the SVI features extracted using algorithm 3 for tree species classification was considerably higher than that extracted using algorithms 1 and 2.

3.5. OFS classification accuracy analysis

Using a window size of 43 × 43 to extract textures and algorithm 3 to calculate SVIs, when 187 features were involved in the classification, the accuracy of tree species discrimination achieved the highest value. Therefore, the MFS containing 187 features was the OFS for tree species discrimination. Fig. 6 shows the fitted histogram of producer and user accuracies obtained using the OFS for tree species classification.

From Fig. 6 and the actual data, using the OFS for 32 greening tree species discrimination, the producer accuracies varied from 81.43% (lowest producer accuracy, T7) to 99.93% (highest producer accuracy, T11). The user accuracies ranged from 69.59% (lowest user accuracy, T24) to 100.00% (highest user accuracy, T3). Except for T24 (69.59%), T25 (72.39%), T26 (77.05%), T29 (76.94%), and T31 (73.49%), the user accuracies of all the other tree species remained high. Except for T6, T24, T25, T26, T29, T31, and T32, the producer and user accuracies of all the other tree species had a minimal difference. In general, a satisfactory recognition result was obtained when the OFS was used for tree species classification.

3.6. Comparison of the effectiveness of tree species discrimination

Fig. 7(a) and (b) show the producer and user accuracies in spider-web graphs generated by the OFSs (supported by the three algorithms) and the MFS classification results under the 43 × 43 texture extraction window, respectively, and their tree species identification maps are presented in Fig. 8(b) and 8(e).

Fig. 7(a) shows that the difference in the producer accuracy among the OFSs and MFS for the tree species classification was extremely small. The discrimination effect of T6, T10, T13, T15, T16, T28, T29, and T32 when using OFS 3 was slightly better than that when using other feature sets. Moreover, the discrimination effect of T5, T9, and T30 when using OFS 3 was slightly worse than that when using other feature sets. For user accuracy (Fig. 7(b)), the discrimination effect of T4, T5, T8, T9, T12, T25, and T27 when using OFS 3 was slightly better than that when using other feature sets. Moreover, the discrimination effect of tree species T13, T15, and T19 when using OFS 3 was slightly worse than that when using other feature sets.

Overall, the curve shapes trend of producer and user accuracies generated from the four types of datasets in tree species classification was relatively similar on the spider-web graphs. The OFS supported by the algorithm 3 construction was better than the other feature sets in the tree species recognition.

Fig. 8(a) shows the true distribution of the patches of tree species in the study area. The results of discriminating them using the OFSs and MFS demonstrated a high degree of consistency with their actual distribution. However, some tree species were incorrectly classified at the edges and inside of the patches. For example, in Fig. 8(b)-8(e), parts of T1, T7, and T16 were mistakenly identified as T24 and T25, T6, and T4, respectively. Some slight differences were observed in the tree species identification results when using the four types of datasets. However, their overall effects on tree species identification were consistent and satisfactory.

4. Discussion

When extracting texture under the most suitable window, the number of features in the OFSs for tree species classification was considerably larger than that in the optimal texture feature sets obtained by extracting texture under nonoptimal windows (Figs. 4 and 5, Table 4). Previous studies have concluded that in tree species recognition based on high-dimensional data, an optimal tree species identification feature set with a few features can be obtained via feature optimization [2,56]. When the window for texture extraction was relatively small, the results obtained in this study were consistent with those of previous studies. However, when the window of texture extraction was relatively large, the results differed considerably from those of previous studies. A possible reason for this is that texture extraction in a small window cannot result in high-accuracy tree species classification, and the presence of a few features can result in tree species discrimination accuracy reaching the upper limit. To extract texture under an optimal large window, more features must be considered in decision-making to increase the accuracy of tree species classification to the upper limit. The findings of this study suggest that the optimal large window could be utilized for texture extraction in multitype feature–based tree species identification.

The cumulative distribution of SVIs in the MFS (Fig. 3), accuracy of tree species classification (Fig. 5, Tables 5 and 6), and number of features selected in the OFSs (Table 4) of the SVI extracted using algorithm 3 were better than those obtained using the remaining two algorithms. In addition, algorithms 1 and 2 exhibit large randomness in the SVI features of the OFSs under different texture windows (Table 4). The number of SVI features extracted using algorithms 1 and 2 in the OFSs is 0 under the 9 × 9 window. This finding indicates that the number of image features contained in the OFSs decreases with the increasing importance of texture features in tree

Table 6
Situation of the SVI feature sets for tree species classification.

Algorithm used	Overall accuracy %	Kappa coefficient
Algorithm 1	55.59	0.5401
Algorithm 2	55.80	0.5422
Algorithm 3	57.18	0.5567

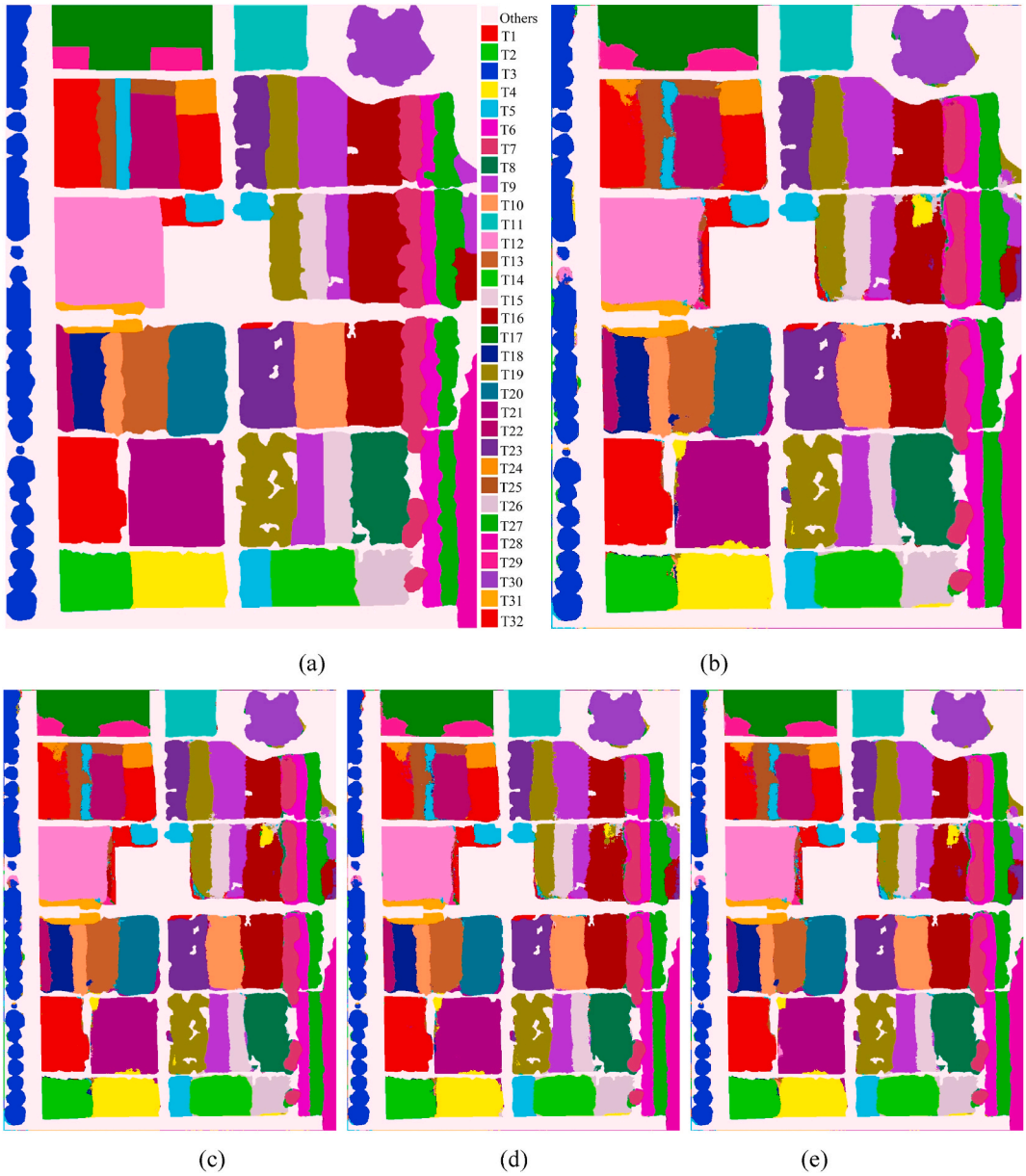

Fig. 8. Tree species discrimination maps of different feature sets. (a) Ground truth; (b) classification result of OFS 1; (c) classification result of OFS 2; (d) classification result of OFS 3; and (e) classification result of MFS.

species classification and that the SVIs extracted using the two algorithms were not satisfactory, resulting in no SVI features being selected. This reveals that algorithms 1 and 2 are not superior to algorithm 3.

The performance of the SVIs extracted with a relative volume constraint in tree species classification was better than that of the SVIs extracted without volume constraints. Algorithm 2 (texture extracted under the 43 × 43 window) was better than algorithm 1 in terms of the evaluation of the cumulative distribution of feature importance, accuracy of tree species classification, and number of SVIs

included in the OFS. The comparison between algorithms 3 and 1 also shows that the SVIs extracted with a relative volume constraint are considerably helpful for tree species classification. These results indicate that the SVI extracted with relative volume constraints exhibits satisfactory performance in the case of tree species discrimination. The SVI extracted by constraining the cylinder volume can improve the accuracy of tree species classification, probably because the volume constraint makes the differences between various tree species obvious. The effect of the variable constraint is better than that of the constant constraint, probably because the variable constraint makes the spectral volume difference of the same tree species consistent at different pixel positions and increases the spectral volume difference of different tree species. However, the constant constraint fails to consider the variation of different pixels with respect to the same tree species in different bands, and the calculated spectral volume may make the same tree species have certain differences.

Herein, the SVI extracted using algorithm 3 exhibits excellent performance. Taking this as an example, when the texture was extracted under small windows (3×3 and 9×9), most of the important SVI variables in the OFSs could be found in the OFS determined by extracting textures under a large window (43×43) (Table 4); however, some changes were present in the importance order. This finding shows that the important SVIs in tree species recognition are deterministic rather than random. We can determine the SVIs that are useful in tree species identification from multiple experiments, and these variables can be directly selected in subsequent studies.

The window size of texture extraction affects the performance of SVIs in tree species classification. When extracting textures under nonoptimal windows, the accuracy of tree species classification of the original MFS with SVIs is lower than that without SVIs (Table 5). When extracting textures under the optimal window and adding the SVI feature to the original MFS, the accuracies of tree species recognition of the three types of feature sets (92.18%, 92.55%, and 92.44%) were higher than that of the original MFS (92.16%) (Table 5). This finding shows that the most suitable window for texture feature extraction can make the real performance of SVIs well displayed in tree species classification. A possible reason for this is that a certain correlation exists among the extracted SVI features. When the texture performance is not very strong, a severe Hughes phenomenon occurs, inhibiting the excellent tree species identification performance of the feature set. However, when the texture performance becomes stronger, the severe Hughes phenomenon is eliminated. This result indicates that suitable large windows should be used to extract texture features in tree species discrimination.

Feature optimization seems to be crucial in tree species classification based on high-dimensional mixed features. As shown in Fig. 4 and Table 5, whether the texture feature is extracted under a small window or a suitable large window, after the SVI feature is incorporated, the accuracy of tree species classification is not as high as that of the OFS obtained after feature optimization. These experimental results show that in tree species discrimination based on high-dimensional mixed features, the features that are beneficial for tree species classification should be screened, and negative features should be eliminated. After removing some features with high correlation and little use, the mapping of tree species can be improved to a certain extent.

Herein, data were collected from two dormancy periods of some tree species (i.e., spring and winter). During these two periods, the spectral reflectance information of patches where dormant tree species are located mainly reflects the comprehensive effect of the spectral reflectance of ground objects, such as tree trunks, fallen leaves, and soil background. Combining SVI features for tree species identification is reasonable and effective when the underlying surface environment of a tree species remains the same. However, when the underlying surface environment is highly heterogeneous, the volume of prisms formed by the spectral curves of same tree species may show large differences and introducing SVI features for tree species classification may result in large errors. Therefore, introducing SVI features for tree species classification requires consideration of similarities and differences in the stand environment where the same dormant tree species are located.

In this study, only one small study area was considered, and a preliminary test was performed using single-type imagery from four periods. Whether the use of more time-series RS data in other regions could obtain similar results is worth discussing. In the future, other RS data will be obtained from additional periods and tested in additional areas, and whether some SVI features can always improve the accuracy of tree species identification, which bands calculated by SVIs play a key role, and why these SVIs are conducive for tree species discrimination will be gradually discovered.

5. Conclusions

Herein, general and improved expressions for SVIs were developed by considering the spectral reflection value, wavelength, and time as parameters. Data were obtained by applying RedEdge-MX to four phases, the SVI extracted using the three algorithms was used for tree species discrimination, and an RF algorithm was employed to preliminarily test if the SVI can promote tree species recognition and which algorithm has better performance. The following conclusions were derived from this study.

(1) The SVI extracted with volume constraints had better performance in tree species discrimination than the SVI extracted without volume constraints. The performance of the SVI extracted with the variable-constrained volume was better than that extracted with the constant-constrained volume.
(2) Combining SVI features with other features could improve the accuracy of tree species discrimination; however, the improvement was limited.
(3) The window size of texture extraction affected the performance of SVIs in tree species classification. Extracting textures and building the MFS with a suitable large window could maximize the importance of SVIs.
(4) Useful SVI features appearing in the OFS were generally deterministic rather than random.

This study reports that SVIs could be incorporated into image feature sets in tree species classification to promote the tree species

identification effect. In particular, in pure forest tree species classification, only used the mixed features of the SB, texture, and DSM (without combining SVI features) could achieve high classification accuracy. It seems unnecessary to combine the SVIs with the mixed features to classify tree species. However, for non-pure forest species discrimination, whether an MFS combined with SVI features can greatly promote the discrimination effect needs further exploration.

Author contribution statement

Huaipeng Liu: Conceived and designed the experiments; Performed the experiments; Analyzed and interpreted the data; Contributed reagents, materials, analysis tools or data; Wrote the paper.

Funding statement

This work was supported by the National Natural Science Foundation of China (Grant No. 32001250) and the Natural Science Foundation of Henan Province, China (Grant No. 202300410293).

Data availability statement

Data will be made available on request.

Additional information

No additional information is available for this study.

Declaration of competing interest

The authors declare that they have no known competing financial interests or personal relationships that could have appeared to influence the work reported in this paper.

Acknowledgements

I want to express my gratitude to the editors and anonymous reviewers.

References

[1] R. Pu, Mapping tree species using advanced remote sensing technologies: a state-of-the-art review and perspective, J. Remote Sens. (2021), 9812624, https://doi.org/10.34133/2021/9812624.
[2] H. Liu, Classification of Tree Species Using UAV-Based Multi-Spectral and Multi-Seasonal Images: a Multi-Feature-Based Approach, New for, 2023, https://doi.org/10.1007/s11056-023-09974-w.
[3] D. Yin, L. Wang, How to assess the accuracy of the individual tree-based forest inventory derived from remotely sensed data: a review, Int. J. Rem. Sens. 37 (19) (2016) 4521–4553, https://doi.org/10.1080/01431161.2016.1214302.
[4] F.E. Fassnacht, H. Latifi, K. Stereńczak, A. Modzelewska, M. Lefsky, L.T. Waser, C. Straub, A. Ghosh, Review of studies on tree species classification from remotely sensed data, Remote Sens. Environ. 186 (2016) 64–87, https://doi.org/10.1016/j.rse.2016.08.013.
[5] P. Gong, R.L. Pu, B. Yu, Conifer species recognition with seasonal hyperspectral data, J. Remote Sens. 2 (1998) 211–217.
[6] B.W. Heumann, An object-based classification of mangroves using a hybrid decision tree- support vector machine approach, Rem. Sens. 3 (11) (2011) 2440–2460, https://doi.org/10.3390/rs3112440.
[7] M. Kamal, S. Phinn, K. Johansen, Object-based approach for multi-scale mangrove composition mapping using multi-resolution image datasets, Rem. Sens. 7 (4) (2015) 4753–4783, https://doi.org/10.3390/rs70404753.
[8] M. Immitzer, C. Atzberger, T. Koukal, Tree species classification with random forest using very high spatial resolution 8-band WorldView-2 satellite data, Rem. Sens. 4 (9) (2012) 2661–2693, https://doi.org/10.3390/rs4092661.
[9] R. Pu, S. Landry, A comparative analysis of high resolution IKONOS and WorldView-2 imagery for mapping urban tree species, Remote Sens. Environ. 124 (2012) 516–533, https://doi.org/10.1016/j.rse.2012.06.011.
[10] K.Y. Peerbhay, O. Mutanga, R. Ismail, Investigating the capability of few strategically placed WorldView-2 multispectral bands to discriminate forest species in kwazulu-natal, South Africa, IEEE J. Sel. Top. Appl. Earth Obs. Rem. Sens. 7 (1) (2013) 307–316, https://doi.org/10.1109/JSTARS.2013.2262634.
[11] T. Wang, H. Zhang, H. Lin, C. Fang, Textural-spectral feature-based species classification of mangroves in mai po nature reserve from Worldview-3 imagery, Rem. Sens. 8 (1) (2016) 24, https://doi.org/10.3390/rs8010024.
[12] M.P. Ferreira, F.H. Wagner, L.E.O.C. Aragão, Y.E. Shimabukuro, C.R.D.S. Filho, Tree species classification in tropical forests using visible to shortwave infrared WorldView-3 images and texture analysis, ISPRS J. Photogrammetry Remote Sens. 149 (2019) 119–131, https://doi.org/10.1016/j.isprsjprs.2019.01.019.
[13] M.A. Cho, R. Mathieu, G.P. Asner, L. Naidoo, J. van Aardt, A. Ramoelo, P. Debba, K. Wessels, R. Main, I.P.J. Smit, B. Erasmus, Mapping tree species composition in south african savannas using an integrated airborne spectral and LiDAR system, Remote Sens. Environ. 125 (10) (2012) 214–226, https://doi.org/10.1016/j.rse.2012.07.010.
[14] L. Naidoo, M.A. Cho, R. Mathieu, G.P. Asner, Classification of savanna tree species, in the Greater Kruger National Park region, by integrating hyperspectral and LiDAR data in a Random Forest data mining environment, ISPRS J. Photogrammetry Remote Sens. 69 (3) (2012) 167–179, https://doi.org/10.1016/j.isprsjprs.2012.03.005.
[15] L.J. Liu, Y. Pang, W.Y. Fan, Z.Y. Li, D.R. Zhang, M.Z. Li, Fused airborne LiDAR and hyperspectral data for tree species identification in natural temperate forest, J. Remote Sens. 17 (3) (2013) 679–695.
[16] H. Torabzadeh, R. Leiterer, A. Hueni, M. Schaepman, F. Morsdorf, Tree species classification in a temperate mixed forest using a combination of imaging spectroscopy and airborne laser scanning, Agric. For. Meteorol. 279 (2019), 107744, https://doi.org/10.1016/j.agrformet.2019.107744.
[17] J.A. Richards, X. Jia, Using suitable neighbors to augment the training set in hyperspectral maximum likelihood classification, Geosci. Rem. Sens. Lett. IEEE 5 (4) (2008) 774–777, https://doi.org/10.1109/LGRS.2008.2005512.

[18] Z. Zhang, A. Kazakova, L.M. Moskal, D.M. Styers, Object-based tree species classification in urban ecosystems using LiDAR and hyperspectral data, Forests 7 (6) (2016) 122, https://doi.org/10.3390/f7060122.
[19] N. Kureel, J. Sarup, S. Matin, S. Goswami, K. Kureel, Modelling vegetation health and stress using hypersepctral remote sensing data, Model. Earth Syst. Environ. 8 (2022) 733–748, https://doi.org/10.1007/s40808-021-01113-8.
[20] D. Li, Y. Ke, H. Gong, X. Li, Object-based urban tree species classification using bi-temporal WorldView-2 and WorldView-3 images, Rem. Sens. 7 (12) (2015) 16917–16937, https://doi.org/10.3390/rs71215861.
[21] H. Liu, H. An, B. Wang, Q. Zhang, Tree species classification using WorldView-2 images based on recursive texture feature elimination, J. Beijing For. Univ. 37 (8) (2015) 53–59, https://doi.org/10.13332/j.1000-1522.20140311.
[22] C.C. Dymond, D.J. Mladenof, V. Radelof, Phenological differences in tasseled cap indices improve deciduous forest classification, Remote Sens. Environ. 80 (3) (2002) 460–472, https://doi.org/10.1016/S0034-4257(01)00324-8.
[23] M.L. Clark, J. Buck-Diaz, J. Evens, Mapping of forest alliances with simulated multi-seasonal hyperspectral satellite imagery, Remote Sens. Environ. 210 (2018) 490–507, https://doi.org/10.1016/j.rse.2018.03.021.
[24] H. Hamraz, N.B. Jacobs, M.A. Contreras, C. Clark, Deep learning for conifer/deciduous classification of airborne LiDAR 3D point clouds representing individual trees, ISPRS J. Photogrammetry Remote Sens. 158 (2019) 219–230, https://doi.org/10.1016/j.isprsjprs.2019.10.011.
[25] C. Masemola, M.A. Cho, A. Ramoelo, Assessing the effect of seasonality on leaf and canopy spectra for the discrimination of an alien tree species, acacia mearnsii, from co-occurring native species using parametric and nonparametric classifiers, IEEE Trans. Geosci. Rem. Sens. 57 (8) (2019) 5853–5867, https://doi.org/10.1109/TGRS.2019.2902774.
[26] Y.F. Shi, T.J. Wang, A.K. Skidmore, M. Heurich, Improving LiDAR-based tree species mapping in Central European mixed forests using multi-temporal digital aerial colour-infrared photographs, Int. J. Appl. Earth Obs. Geoinf. 84 (2020), 101970, https://doi.org/10.1016/j.jag.2019.101970.
[27] C. Masemola, M.A. Cho, A. Ramoelo, Sentinel-2 time series based optimal features and time window for mapping invasive australian native acacia species in kwazulu natal, South Africa, Int. J. Appl. Earth Obs. Geoinf. 93 (2020), 102207, https://doi.org/10.1016/j.jag.2020.102207.
[28] R. Pu, S. Landry, Mapping urban tree species by integrating multi-seasonal high resolution Pléiades satellite imagery with airborne LiDAR data, Urban For. Urban Gree. 53 (2020), 126675, https://doi.org/10.1016/j.ufug.2020.126675.
[29] J.H. Zhou, Y.F. Zhou, W.S. Mu, Mathematic descriptor for identifying plant species: a case study on urban landscape vegetation, J. Remote Sens. 15 (3) (2011) 524–538.
[30] M. Åkerblom, P. Raumonen, R. Mäkipää, M. Kaasalainen, Automatic tree species recognition with quantitative structure models, Remote Sens. Environ. 191 (2017) 1–12, https://doi.org/10.1016/j.rse.2016.12.002.
[31] X. Yu, J. Hyyppä, P. Litkey, H. Kaartinen, M. Vastaranta, M. Holopainen, Single-sensor solution to tree species classification using multispectral airborne laser scanning, Rem. Sens. 9 (2) (2017) 108, https://doi.org/10.3390/rs9020108.
[32] S. Tuominen, R. Näsi, E. Honkavaara, A. Balazs, T. Hakala, N. Viljanen, I. Polonen, H. Saari, H. Ojanen, Assessment of classifiers and remote sensing features of hyperspectral imagery and stereo-photogrammetric point clouds for recognition of tree species in a forest area of high species diversity, Rem. Sens. 10 (5) (2018) 714, https://doi.org/10.3390/rs10050714.
[33] M.D. Cross, T. Scambos, F. Pacifici, W.E. Marshall, Determining effective meter-scale image data and spectral vegetation indices for tropical forest tree species differentiation, IEEE J. Sel. Top. Appl. Earth Obs. Rem. Sens. 12 (8) (2019) 2934–2943, https://doi.org/10.1109/JSTARS.2019.2918487.
[34] M. Immitzer, M. Neuwirth, S. Böck, H. Brenner, F. Vuolo, C. Atzberger, Optimal input features for tree species classification in central europe based on multi-temporal sentinel-2 data, Rem. Sens. 11 (22) (2019) 2599, https://doi.org/10.3390/rs11222599.
[35] B. Apostol, M. Petrila, A. Lorenț, A. Ciceu, V. Gancz, O. Badea, Species discrimination and individual tree detection for predicting main dendrometric characteristics in mixed temperate forests by use of airborne laser scanning and ultra-high-resolution imagery, Sci. Total Environ. 698 (2020), 134074, https://doi.org/10.1016/j.scitotenv.2019.134074.
[36] J.P. Ardila, V.A. Tolpekin, W. Bijker, A. Stein, Markov-random-field-based super-resolution mapping for identification of urban trees in VHR images, ISPRS J. Photogrammetry Remote Sens. 66 (6) (2011) 762–775, https://doi.org/10.1016/j.isprsjprs.2011.08.002.
[37] A. Ghosh, P.K. Joshi, A comparison of selected classification algorithms for mapping bamboo patches in lower gangetic plains using very high resolution WorldView-2 imagery, Int. J. Appl. Earth Obs. Geoinf. 26 (1) (2014) 298–311, https://doi.org/10.1016/j.jag.2013.08.011.
[38] C. Lin, S.C. Popescu, G. Thomson, K. Tsogt, C.I. Chang, Classification of tree species in overstorey canopy of subtropical forest using QuickBird images, PLoS One 10 (5) (2015), e0125554, https://doi.org/10.1371/journal.pone.0125554.
[39] D. Harrison, B. Rivard, A. Sánchez-Azofeifa, Classification of tree species based on longwave hyperspectral data from leaves, a case study for a tropical dry forest, Int. J. Appl. Earth Obs. Geoinf. 66 (2018) 93–105, https://doi.org/10.1016/j.jag.2017.11.009.
[40] A. Modzelewska, F.E. Fassnacht, K. Stereńczak, Tree species identification within an extensive forest area with diverse management regimes using airborne hyperspectral data, Int. J. Appl. Earth Obs. Geoinf. 84 (2020), 101960, https://doi.org/10.1016/j.jag.2019.101960.
[41] H. Liu, H. An, Urban greening tree species classification based on HSV colour space of WorldView-2, J. Indian Soc. Remote Sens. 47 (11) (2019) 1959–1967, https://doi.org/10.1007/s12524-019-01028-z.
[42] W.W. Shi, Y.H. Gong, X.Y. Tao, D. Cheng, N.N. Zheng, Fine-grained image classification using modified DCNNs trained by cascaded softmax and generalized large-margin losses, IEEE Transact. Neural Networks Learn. Syst. 30 (3) (2019) 683–694, https://doi.org/10.1109/TNNLS.2018.2852721.
[43] H.B. Zhang, D.D. Qiu, R.Z. Wu, Y.X. Deng, D.H. Ji, T. Li, Novel framework for image attribute annotation with gene selection XGBoost algorithm and relative attribute model, Appl. Soft Comput. 80 (2019) 57–79, https://doi.org/10.1016/j.asoc.2019.03.017.
[44] L.H. Zhong, L.N. Hu, H. Zhou, Deep learning based multi-temporal crop classification, Remote Sens. Environ. 221 (2019) 430–443, https://doi.org/10.1016/j.rse.2018.11.032.
[45] J.N. Niu, Y.M. Sun, Y.R. Zhang, Y.F. Ji, Noise-suppressing channel allocation in dynamic DWDM-QKD networks using LightGBM, Opt Express 27 (22) (2019) 31741–31756, https://doi.org/10.1364/OE.27.031741.
[46] A. Kemal, K. Serhat, C. Onur, Classification and diagnosis of cervical cancer with stacked autoencoder and softmax classification, Expert Syst. Appl. 115 (2019) 557–564, https://doi.org/10.1016/j.eswa.2018.08.050.
[47] M.P. Ferreira, M. Zortea, D.C. Zanotta, Y.E. Shimabukuro, C.R.D.S. Filho, Mapping tree species in tropical seasonal semi-deciduous forests with hyperspectral and multispectral data, Remote Sens. Environ. 179 (2016) 66–78, https://doi.org/10.1016/j.rse.2016.03.021.
[48] J. Maschler, C. Atzberger, M. Immitzer, Individual tree crown segmentation and classification of 13 tree species using airborne hyperspectral data, Rem. Sens. 10 (8) (2018) 1218, https://doi.org/10.3390/rs10081218.
[49] H. Liu, H. An, Analysis of the importance of five new spectral indices from WorldView-2 in tree species classification, Spatial Sci. 65 (3) (2020) 455–466, https://doi.org/10.1080/14498596.2018.1521754.
[50] H. Liu, Effectiveness of the spectral area index created by three algorithms for tree species recognition, Ann. For. Sci. 80 (2023) 17, https://doi.org/10.1186/s13595-023-01184-w.
[51] H. Liu, H. An, Extraction of four types of urban ground objects based on a newly created WorldView-2 multi-colour spectral index, J. Indian Soc. Remote Sens. 48 (7) (2020) 1091–1100, https://doi.org/10.1007/s12524-020-01134-3.
[52] H. Liu, X. Zuo, Extraction of blue roofs using BRSAM and the newly created spectral index derived from WorldView-2/3 imagery, Heliyon 8 (9) (2022), e10417, https://doi.org/10.1016/j.heliyon.2022.e10417.
[53] H. Liu, Classification of urban tree species using multi-features derived from four-season RedEdge-MX data, Comput. Electron. Agric. 194 (2022), 106794, https://doi.org/10.1016/j.compag.2022.106794.

[54] A. Agarwal, S. Kumar, D. Singh, An adaptive technique to detect and remove shadow from drone data, J. Indian Soc. Remote Sens. 49 (2021) 491–498, https://doi.org/10.1007/s12524-020-01227-z.
[55] S. Van der Linden, A. Rabe, M. Held, B. Jakimow, P.J. Leitão, A. Okujeni, M. Schwieder, S. Suess, P. Hostert, The EnMAP-Box- A Toolbox and application programming interface for EnMAP data processing, Rem. Sens. 7 (9) (2015) 11249–11266, https://doi.org/10.3390/rs70911249.
[56] R. Pu, L. Shawn, Q. Yu, Assessing the potential of multi-seasonal high resolution pléiades satellite imagery for mapping urban tree species, Int. J. Appl. Earth Obs. Geoinformation. 71 (2018) 144–158, https://doi.org/10.1016/j.jag.2018.05.005.